Synthesis and electrochemical properties of α-Fe₂O₃ particles for energy storage devices

Bui Thi Hang[*], Tran Van Dang

International Training Institute for Materials Science, Hanoi University of Science and Technology (HUST), No. 1 Dai Co Viet Road, Hai Ba Trung, Ha Noi, Viet Nam

[*]Emails: *hang@itims.edu.vn, hang.buithi@hust.edu.vn*

Abstract. In this study, we fabricated α-Fe₂O₃ materials via a facile hydrothermal route to use as the active material for the anode of an iron-based battery. The particle size of α-Fe₂O₃ was in a range of a few hundreds of nanometers to a few micrometers. The structural characteristics and particle size of the synthesized iron oxides were studied via X-ray diffraction (XRD) and scanning electron microscopy (SEM). The electrochemical behavior of iron oxide electrode was investigated by cyclic voltammetry (CV). The distribution of iron species was observed by Energy dispersive X-ray spectroscopy (EDS) measurement. Carbon was used as an additive to improve the conductivity of α-Fe₂O₃/C composite electrode. The electrochemical measurements revealed that the prepared α-Fe₂O₃ particles provided good cyclability. The EDS results showed that iron species were dispersed on the carbon surface during discharge-discharge through the electrochemical dissolution-deposition process of iron.

Keywords: α-Fe₂O₃ particles, Fe₂O₃/C composite electrode, hydrothermal method, iron-based battery.

Classification numbers: 2.4,2.8, 2.8.2, 2.9.4.

1. INTRODUCTION

In recent years, rechargeable iron-based batteries have received considerable attention due to their high theoretical capacity, long cycle life, high electrochemical stability, low cost, and environmental safety [1]. Thus, iron electrodes have received great attention [2–8]. The overall electrochemical behavior involved in the passivation and dissolution of iron in alkaline solution was proposed earlier [9, 10] containing two main steps, the first of which is:

$$\text{Fe} + 2\text{OH}^- \quad \rightleftharpoons \quad \text{Fe(OH)}_2 + 2e \qquad (1)$$

$$(\text{E}^0 = -0.978 \text{ V vs. Hg/HgO}) \text{ [9]}$$

The second oxidation step of iron electrode involves:

$$\text{Fe(OH)}_2 + \text{OH}^- \quad \rightleftharpoons \quad \text{FeOOH} + \text{H}_2\text{O} + e \qquad (2)$$

$$(\text{E}^0 = -0.658 \text{ V vs. Hg/HgO [9]}$$

and/or

$$3Fe(OH)_2 + 2OH^- \rightleftharpoons Fe_3O_4.4H_2O + 2e \quad\quad (3)$$

$$(E^0 = -0.758 \text{ V vs. Hg/HgO } [10]$$
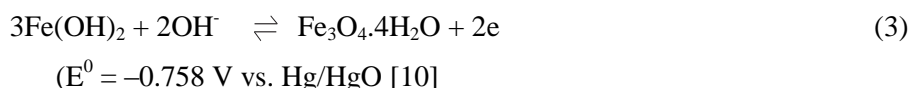
However, the problem of iron electrodes is that there is a passive layer of $Fe(OH)_2$ formed during the cycling leading to a low utilization coefficient. Further, the potential of the reduction reaction $Fe/Fe(OH)_2$ is only slightly more negative than that of the hydrogen evolution in an alkaline solution, thereby there is a simultaneous evolution of hydrogen during charging [2,11 - 14]. This is the cause of the low charge/discharge efficiency and high self-discharge rate of iron electrodes [12]. To overcome the limitations of iron electrodes, a number of additives are incorporated into the iron electrode during the fabrication process or into the electrolyte or both [5, 15 - 20].

Recently, several authors have reported that Fe/carbon mixed composite electrodes, using various kinds of carbons as additives, showed improved passivation, charge-discharge performance of iron electrodes [21 - 23].

In our present study, α-Fe₂O₃ polyhedral particles ranging in size from a few hundreds of nanometers to a few micrometers were prepared and used as the active material of an iron-based battery anode. Nanocarbons were used as the additive to improve the electrode conductivity and the cyclability of iron oxide electrode. The electrochemical properties of iron oxide carbon electrodes were investigated by electrochemical measurements in an alkaline aqueous electrolyte.

2. MATERIALS AND METHODS

α-Fe₂O₃ materials were prepared via a facile hydrothermal route. Iron chloride ($FeCl_3.6H_2O$) was used as an iron source and cetyltrimethylammonium bromide (CTAB) was used as a surfactant. Initially, CTAB was dissolved in deionized water to form an aqueous solution with a concentrations of 0.04 M. The mixture was stirred until the solution became transparent. An iron chloride aqueous solution with a concentration of 0.02 M was prepared using the same process. Next, 80 mL of the iron chloride aqueous solution was dissolved in 80 mL of the CTAB aqueous solution, which was then stirred for 60 min to form a homogeneous solution. The resulting solution was transferred into a Teflon-lined stainless-steel autoclave, sealed, and maintained at 190 °C for 6 h following a typical hydrothermal process. The autoclave was then gradually cooled down to room temperature. The red brown precipitates were collected through centrifugation, washed several times with distilled water and ethanol, subsequently dried at 60 °C for 12 h, and finally annealed at 400 °C for 2 h in air to obtain α-Fe₂O₃ powder.

The crystal structure of the synthesized powder was studied using an X-ray diffractometer (XRD; Rigaku), measured with Cu Kα radiation (k = 0.1542 nm, 40 kV, 150 mA) at a scanning speed of 2°/min over a scan range of angle from 20° to 80°. The morphology of the as-prepared materials were observed by scanning electron microscopy (SEM) using a JSM-6060LA/VI analytical scanning electron microscope (JEOL).

To determine the electrochemical behavior of the as-prepared Fe₂O₃, we prepared an electrode sheet by mixing 45 wt.% acetylene black (AB) as additive, 45 wt.% Fe₂O₃ powder as active material and 10 wt.% polytetrafluoroethylene (PTFE; Daikin Co.) as binder followed by rolling. Each electrode was made in the form of a pellet with a diameter of 1 cm.

Cyclic voltammetry (CV) measurements were carried out in three-electrode glass cells with Fe_2O_3/AB composite electrode as the working electrode, Pt mesh as the counter-electrode, and Hg/HgO as the reference electrode. The electrolyte was 8 mol dm^{-3} KOH aqueous solution. CV measurements were taken at a scan rate of 5 mV s^{-1} and within a range of −1.3 V to −0.1 V. After the 15th redox cycle, the Fe_2O_3/AB composite electrodes were removed, washed with deionized water and dried. The morphology and the distribution of iron and carbon of Fe_2O_3/AB composite electrodes were observed by scanning electron microscopy (SEM) and X-ray energy dispersion spectroscopy (EDS) using a JSM-6060LA/VI analytical scanning electron microscope (JEOL) so as to compare with the results of the electrodes before cycling. The charge/discharge measurement was performed under the following conditions: In the charge course, galvanostatic process with a cutoff capacity of ~1007 mAh g^{-1}-Fe_2O_3 and the charge current density at 50 mA.cm^{-2} were set. In the discharge course, a constant current density of 2.0 mA cm^{-2} was applied with a cutoff potential of −0.1 V. For all electrochemical measurements, we used fresh electrodes without pre-cycling.

3. RESULTS AND DISCUSSION

The XRD pattern of the as-prepared iron oxide is presented in Figure 1. The most typical peaks were characterized by (012), (104), (110), (113), (024), (116), (018), (214), (300), corresponding to the values of 2θ (degree) of about 28.2, 33.12, 35.6, 40.82, 49.41, 54.0, 57.51, 62.38, and 63.95°, respectively in the XRD diagram. They are characteristic of a typical pattern of the α-Fe_2O_3 particles (ICSD No.82135). Consequently, the obtained materials are pure α-Fe_2O_3.

Figure 2 shows SEM images of the α-Fe_2O_3 particles that have a polyhedral shape, and range in size from a few hundreds of nanometers to a few micrometers. Thus, α-Fe_2O_3 microparticles with a polyhedral shape have been successfully prepared by a facile hydrothermal route. They were used as anode active materials in iron-based batteries.

An SEM image of Acetylene black (AB, Denki Kagaku Co.) material is shown in Figure 3. The average diameter of AB is about 50 nm. It was used as an electrode additive in the present work to improve the conductivity and the cyclability of the Fe_2O_3 electrode.
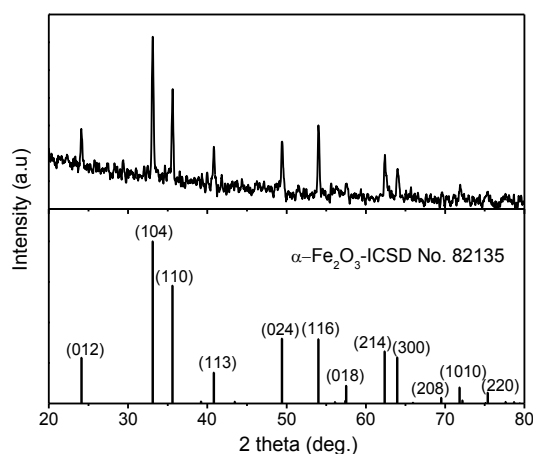
Figure 1. XRD pattern of the α-Fe_2O_3 particles.
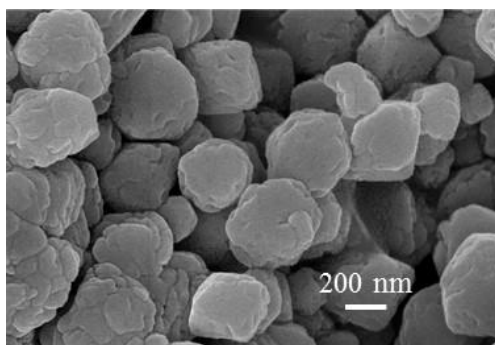
Figure 2. SEM images of the prepared α-Fe$_2$O$_3$ microparticles.
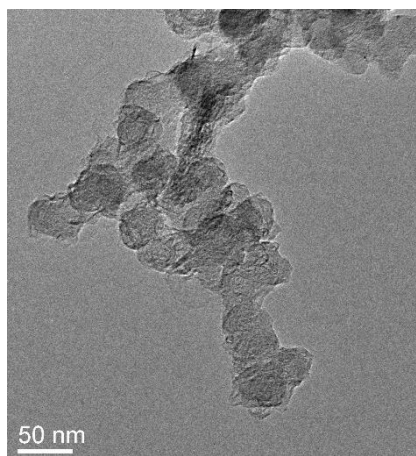
Figure 3. SEM image of AB.

After mixing the synthesized iron oxide and acetylene black (AB), the α-Fe$_2$O$_3$/AB electrode was observed by SEM-EDS measurement and the results are shown in Figure 4. It is clear that α-Fe$_2$O$_3$ particles are distributed on the AB carbon surface. Such a distribution of α-Fe$_2$O$_3$ and AB will support the redox reaction of Fe$_2$O$_3$. A composite anode of active metals with a nano-sized carbon conductor is expected to improve the problems of metal anodes for iron-based batteries.

The cyclic voltammograms of the α-Fe$_2$O$_3$/AB electrodes are shown in Figure 5. Two oxidation peaks are observed at around −0.75 V (a_1) and −0.6 V (a_2) on the forward scan while a reduction peak occurs at around −1.15 V (c_2) on the backward scan. The reduction peak c_1 is overlapped by a hydrogen evolution peak at around −1.2 V (H_2). A previous investigation [24] indicated that the clear surface of iron was never exposed to the electrolyte, and over a partially oxidized surface, adsorption of hydroxyl ion takes place. The dissolution of the oxide or underlying metal by the ion transport through the oxide can also take place.

Theoretically, the first and second anodic peaks (a_1 and a_2) can be attributed to the oxidation of Fe to Fe(II) (Eq. 1) and Fe(II)/Fe(III) (Eq. 2 or 3) while cathodic peaks (c_2 and c_1) correspond to the reduction of Fe(III)/Fe(II) and Fe(II)/Fe, respectively. Thus, a_1 and c_1 correspond to the Fe/Fe(II) redox couple while a_2 and c_2 correspond to the Fe(II)/Fe(III) redox couple. At the first scan, Fe$_2$O$_3$ was converted to Fe(II) (c_2) at a low potential of around −1.1 V and no reduction peak of Fe(II)/Fe (c_1) was observed. The redox current of the Fe(II)/Fe(III)(a_2/c_2) couple was much higher than that of the Fe/Fe(II)(a_1/c_1) couple. With further

cycling, the redox current of the Fe(II)/Fe(III) couple increased, reached stability, and then gradually decreased. This could be ascribed to the insulating nature of the $Fe(OH)_2$ active material formed during cycling. The $Fe(OH)_2$ passive layer caused an increase in overpotential of the Fe/Fe(II) redox couple and consequently the oxidation of Fe to Fe(II)(a_1) took place at a more positive potential. The oxidation peak a_2 contains the oxidation of Fe/Fe(II) and Fe(II)/Fe(III), therefore the redox current of the Fe(II)/Fe(III)(a_2/c_2) couple was much higher than that of the Fe/Fe(II)(a_1/c_1) couple.
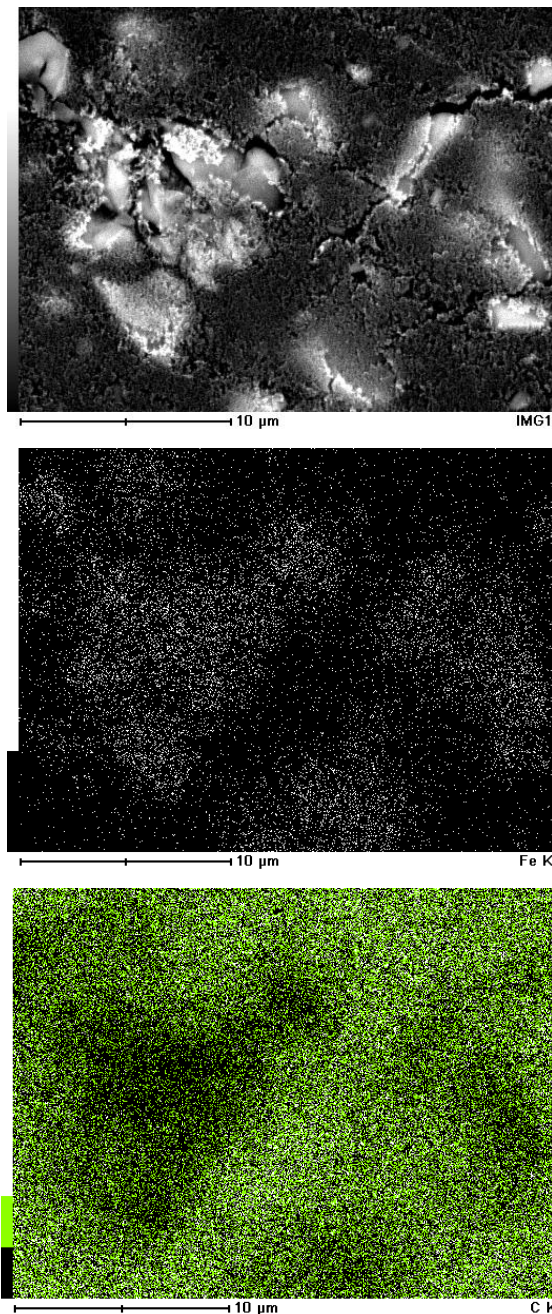
Figure 4. SEM image and distribution of iron and carbon of the α-Fe_2O_3/AB electrode before cycling.
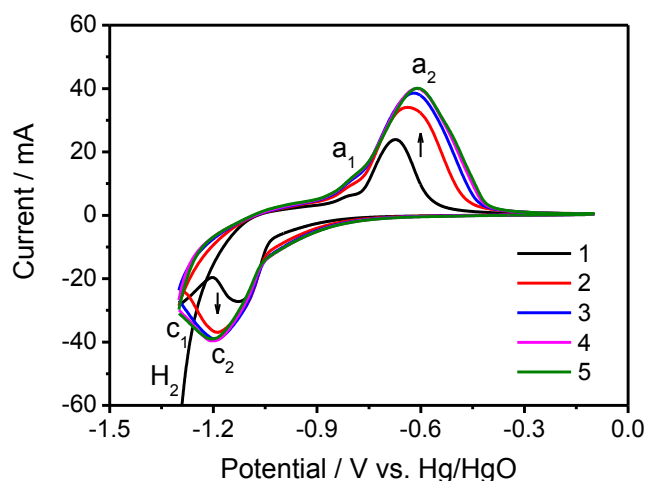
Figure 5. Cyclic voltammograms of Fe$_2$O$_3$/AB composite electrode. (The arrows indicate the change of the current with cycle).

To observe the distribution of iron in the Fe$_2$O$_3$/AB electrode after cycling, SEM-EDS measurements were carried out and the results are shown in Figure 6. After the 15th cycle, iron was more dispersed on the carbon surface via charge–discharge cycles. This dispersion must be due to deposition/dissolution associated with the redox cycles of iron. According to some authors, the formation of Fe(OH)$_2$ proceeds through the formation of intermediate soluble species $HFeO_2^-$ [1,9,12].

$$Fe + OH^- \quad \rightleftharpoons \quad [Fe(OH)]_{ad} + e \qquad (4)$$

$$[Fe(OH)]_{ad} + 2OH^- \quad \rightleftharpoons \quad HFeO_2^- + H_2O + e \qquad (5)$$

and

$$HFeO_2^- + H_2O \rightleftharpoons Fe(OH)_2 + OH^- \qquad (6)$$
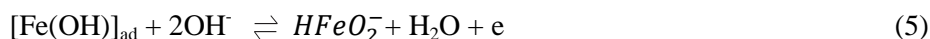
The intermediate soluble species HFeO$_2^-$ plays an important role in iron dispersion in the Fe$_2$O$_3$/AB electrode. During cycling, soluble species $HFeO_2^-$ will be dispersed on the carbon surface via deposition/dissolution mechanism. Such a distribution of iron species will support the redox reaction of iron. Thus, the redox current increased in several initial cycles. To check this supposition, electrochemical impedance spectroscopy (EIS) measurements were carried out on the Fe$_2$O$_3$/AB electrodes before and after cycling at open circuit potential (OCP), the results are presented in Figure 7. Each spectrum consisted of a semicircle in a high frequency region, which was assigned to the interfacial response, followed by a straight line in the lower frequency region corresponding to the Warburg impedance. Before cycling, a semicircle was observed. It may be due to the hydrogen evolution occurring on the surface of electrode causing the corrosion at OCP. After the fifth cycling, the diameter of the semicircle decreased. It suggested that the resistance of electrodes decreased in the initial cycles. This led to an increase in redox current in the above CV measurement.

To evaluate the applicability of the synthesized α-Fe$_2$O$_3$, cycle performance measurements of the Fe$_2$O$_3$/AB electrode were carried out, and the results are shown in Figure 8. The initial discharge capacity was mA.h.g^{-1}, the maximum value reached 405 mA.h.g^{-1} after 2 cycles and then gradually decreased to 120 mA.h.g^{-1} after 30 cycles. Thus, the highest capacity was achieved at the second cycle and then gradually decreased with repeated cycling. The fading

capacity may originate from the aggregation of iron particles during cycling, increasing the resistance of the electrode. With further reseach on preparation methods to control particle shape, morphology and size, α-Fe$_2$O$_3$ is expected to be a potential candidate for use in iron-based battery anode.
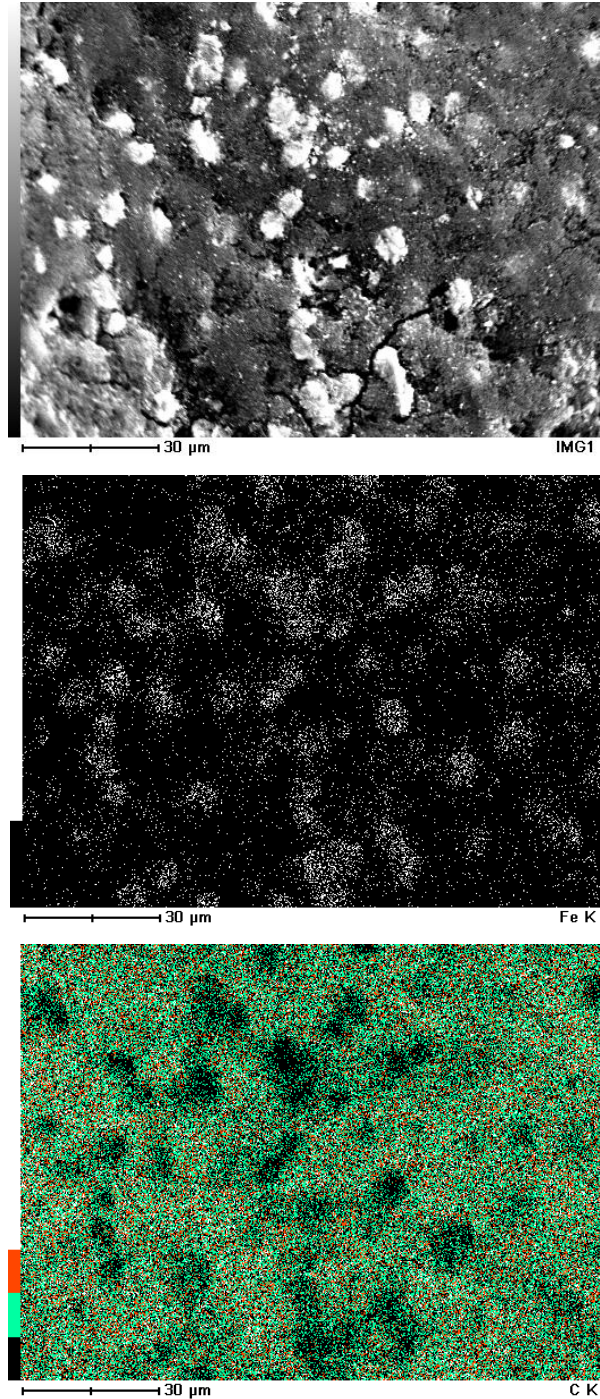
Figure 6. SEM image and distribution of iron and carbon of the α-Fe$_2$O$_3$/AB electrode after the 15th cycle.
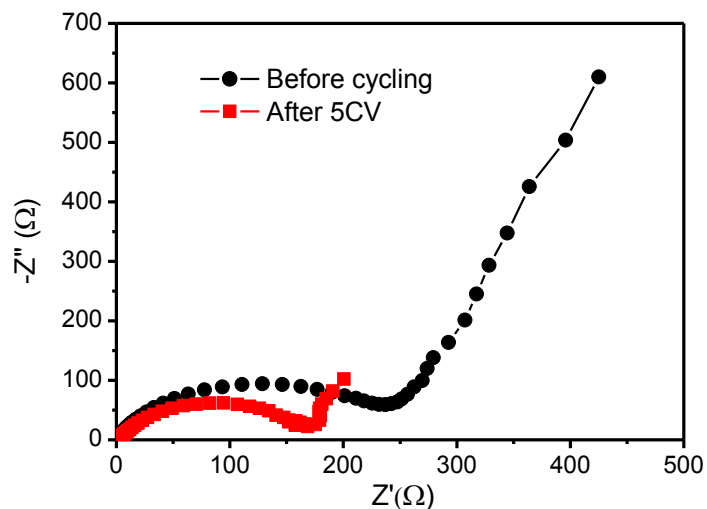
Figure 7. Electrochemical Impedance Spectroscopy (EIS) of the Fe$_2$O$_3$/AB composite electrode in KOH solution.
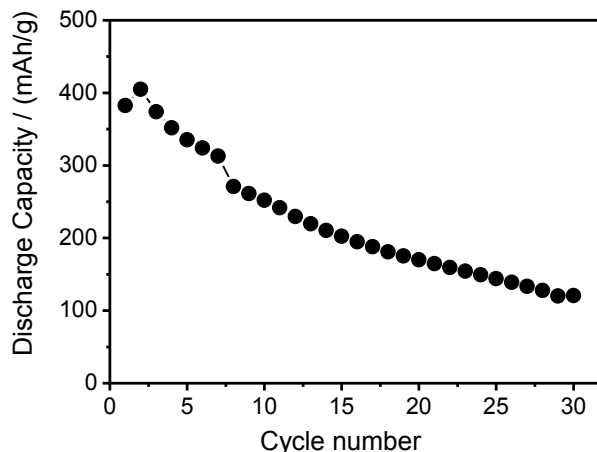
Figure 8. Cycle performance of the Fe$_2$O$_3$/C electrode.

4. CONCLUSIONS

In this work, α-Fe$_2$O$_3$ microparticles with polyhedral shape were synthesized via a facile hydrothermal route and used as anode active material in iron-based batteries. The particle size of α-Fe$_2$O$_3$ is in a range of a few hundreds of nanometers to a few micrometers. Nanocarbon is also applied as an additive to enhance the conductivity of iron oxide electrodes. The electrochemical properties of α-Fe$_2$O$_3$/AB electrodes were investigated. The synthesized α-Fe$_2$O$_3$ materials showed large redox peaks but the deposition peak of iron was covered by hydrogen evolution. The prepared α-Fe$_2$O$_3$ showed improved redox reaction and thus provided good cyclability. Iron species were dispersed on the carbon surface during discharge-discharge through the electrochemical dissolution-deposition process of iron and such a distribution of iron species supported the redox reaction of iron. The synthesized iron oxide material is a potential candidate for iron-based battery anode.

Declaration of competing interest. The authors declare that they have no known competing financial interests or personal relationships that could have appeared to influence the work reported in this paper.

REFERENCES

1. Černý J., Micka K. - Voltammetric study of an iron electrode in alkaline electrolytes, J. Power Sources **25** (1989) 111-122. doi:10.1016/0378-7753(89)85003-7.

2. Posada J. O. G., Hall P. J. - Controlling hydrogen evolution on iron electrodes, Int. J. Hydrogen Energy **41** (2016) 20807-20817. doi:10.1016/j.ijhydene.2016.04.123.

3. Gil Posada J. O., Hall P. J. - Post-hoc comparisons among iron electrode formulations based on bismuth, bismuth sulphide, iron sulphide, and potassium sulphide under strong alkaline conditions, J. Power Sources **268** (2014) 810-815. doi:10.1016/j.jpowsour. 2014.06.126.

4. Yang B., Malkhandi S., Manohar A. K., Surya Prakash G. K., Narayanan S. R. - Organo-sulfur molecules enable iron-based battery electrodes to meet the challenges of large-scale electrical energy storage, Energy Environ. Sci. **7** (2014) 2753. doi:10.1039/C4EE01454E.

5. Shangguan E., F. Li, Li J., Chang Z., Li Q., Yuan X. Z., Wang H. - FeS/C composite as high-performance anode material for alkaline nickel–iron rechargeable batteries, J. Power Sources **291** (2015) 29-39. doi:10.1016/j.jpowsour.2015.05.019.

6. Narayanan S. R., Prakash G. K. S., Manohar A., Yang B., Malkhandi S., Kindler A. - Materials challenges and technical approaches for realizing inexpensive and robust iron–air batteries for large-scale energy storage, Solid State Ionics **216** (2012) 105-109. doi:10.1016/j.ssi.2011.12.002.

7. Sundar Rajan A., Ravikumar M. K., Priolkar K.R ., Sampath S., Shukla A. K. - Carbonyl-Iron Electrodes for Rechargeable-Iron, Electrochem Energy Technol. **1** (2014) 2-9. doi:10.1515/eetech-2014-0002.

8. Malkhandi S., Yang B., Manohar A. K., Prakash G. K. S., Narayanan S. R. - Self-Assembled Monolayers of n -Alkanethiols Suppress Hydrogen Evolution and Increase the Efficiency of Rechargeable Iron Battery Electrodes, J. Am. Chem. Soc. **135** (2013) 347-353. doi:10.1021/ja3095119.

9. Chakkaravarthy C., Periasamy P., Jegannathan S., Vasu K. I. - The nickel/iron battery, J. Power Sources **35** (1991) 21-35. doi:10.1016/0378-7753(91)80002-F.

10. Micka K., Zábranský Z. - Study of iron oxide electrodes in an alkaline electrolyte, J. Power Sources **19** (1987) 315-323. doi:10.1016/0378-7753(87)87007-6.

11. Jayalakshmi N., Muralidharan V. S. - Electrochemical behaviour of iron oxide electrodes in alkali solutions, J. Power Sources **32** (1990) 277-286. doi:10.1016/0378-7753(90)87021-I.

12. Caldas C. A., Lopes M. C., Carlos I. A. - The role of FeS and $(NH4)_2CO_3$ additives on the pressed type Fe electrode, J. Power Sources **74** (1998) 108-112. doi:10.1016/S0378-7753(98)00039-1.

13. Díez-Pérez I., Gorostiza P., Sanz F. - Direct Evidence of the Electronic Conduction of the

Passive Film on Iron by EC-STM, J. Electrochem. Soc. **150** (2003) B348. doi:10.1149/1.1580823.

14. De Koninck M., Bélanger D. - The electrochemical generation of ferrate at pressed iron powder electrode: comparison with a foil electrode, Electrochim Acta. **48** (2003) 1435-1442. doi:10.1016/S0013-4686(03)00021-5.

15. Ravikumar M. K., Rajan A. S., Sampath S., Priolkar K.R., Shukla A. K. - In Situ Crystallographic Probing on Ameliorating Effect of Sulfide Additives and Carbon Grafting in Iron Electrodes, J. Electrochem. Soc. **162** (2015) A2339-A2350. doi:10.1149/2.0721512jes.

16. Figueredo-Rodríguez H. A., McKerracher R. D., Insausti M., Luis A. G., de León C. P., Alegre C., Baglio V., Aricò A. S., Walsh F. C. - A Rechargeable, Aqueous Iron Air Battery with Nanostructured Electrodes Capable of High Energy Density Operation, J. Electrochem. Soc. **164** (2017) A1148-A1157. doi:10.1149/2.0711706jes.

17. Hayashi K., Wada Y., Maeda Y., Suzuki T., Sakamoto H., Tan W. K., Kawamura G., Muto H., Matsuda A. - Electrochemical Performance of Sintered Porous Negative Electrodes Fabricated with Atomized Powders for Iron-Based Alkaline Rechargeable Batteries, J. Electrochem. Soc. **164** (2017) A2049-A2055. doi:10.1149/2.1311709jes.

18. Wu M. C., Zhao T. S., Tan P., Jiang H. R., Zhu X. B. - Cost-effective carbon supported Fe2O3 nanoparticles as an efficient catalyst for non-aqueous lithium-oxygen batteries, Electrochim Acta. **211** (2016) 545-551. doi:10.1016/j.electacta.2016.05.147.

19. Li Y., Lu J. - Metal-Air Batteries: Will They Be the Future Electrochemical Energy Storage Device of Choice?, ACS Energy Lett. **2** (2017). doi:10.1021/acsenergylett. 7b00119.

20. Jiang W., Liang F., Wang J., Su L., Wu Y., Wang L. - Enhanced electrochemical performances of FeOx –graphene nanocomposites as anode materials for alkaline nickel–iron batteries, RSC Adv. **4** (2014) 15394-15399. doi:10.1039/C4RA00018H.

21. Hang B. T., Eashira M., Watanabe I., Okada S., Yamaki J. I., Yoon S. H., Mochida I. - The effect of carbon species on the properties of Fe/C composite for metal-air battery anode, J. Power Sources **143** (2005) 256-264. doi:10.1016/j.jpowsour.2004.11.044.

22. Hang B. T., Watanabe T., Egashira M., Watanabe I., Okada S., Yamaki J. - The effect of additives on the electrochemical properties of Fe/C composite for Fe/air battery anode, J. Power Sources **155** (2006) 461-469. doi:10.1016/j.jpowsour.2005.04.010.

23. Hang B. T., Yoon S. H., Okada S., Yamaki J. - Effect of metal-sulfide additives on electrochemical properties of nano-sized Fe$_2$O$_3$-loaded carbon for Fe/air battery anodes, J. Power Sources **168** (2007) 522-532. doi:10.1016/j.jpowsour.2007.02.067.

24. Kalaignan G. P., Muralidharan V. S., Vasu K. I. - Triangular potential sweep voltammetric study of porous iron electrodes in alkali solutions, J. Appl. Electrochem **17** (1987) 1083-1092. doi:10.1007/BF01024374.